MATERIALS RESEARCH LETTERS

Mater. Res. Lett., 2015
Vol. 3, No. 3, 169–175, http://dx.doi.org/10.1080/21663831.2015.1045630

Taylor & Francis
Taylor & Francis Group

www.tandfonline.com/toc/tmrl20/current

Thermally Induced Interdiffusion and Precipitation in a Ni/Ni_3Al System

C. Sun[a]*, E. Martínez[a], J.A. Aguiar[b], A. Caro[a], J.A. Valdez[a], K. Baldwin[a], Y. Xu[a], B.P. Uberuaga[a], O. Anderoglu[a] and S.A. Maloy[a]

[a]*Los Alamos National Laboratory, Los Alamos, NM 87545, USA;* [b]*National Renewable Energy Laboratory, Golden, CO 80401, USA*

(*Received 3 February 2015; final form 23 March 2015*)

Supplementary Material Available Online

Ordered Ni_3Al intermetallic precipitates constitute the main hardening sources of Ni-based superalloys. Here, we report the interdiffusion and precipitation behavior in a Ni/Ni_3Al model system. The deposition of Ni_3Al on a pure Ni layer at 500°C generated $L1_2$-structured γ' (Ni_3Al) precipitates, preferentially at the interface. After annealing at 800°C for 1 h, interdiffusion between Ni and Ni_3Al layers occurred, and the γ' precipitates that grew near the parent Ni/Ni_3Al interface are $\sim$2.8 times larger in size than those formed in the matrix. Monte Carlo simulations indicate that vacancies preferentially diffuse along the Ni/Ni_3Al interface, increasing the probability of precipitation.

Keywords: Ni-based Superalloy, Interdiffusion, Precipitation, Ni/Ni_3Al Interface, Thermal Annealing

1. Introduction Ni-based superalloys exhibit high strength, long-time rupture strength, and excellent resistance to oxidation at elevated temperatures.[1–3] In Ni-based superalloys, the $L1_2$-structured γ' precipitates ($Ni_3(Al,Ti)$) contribute significantly to the high-temperature strength and the fcc-structured γ matrix can accommodate extensive plastic deformation, resulting in a good combination of high strength and excellent ductility at high temperatures.[4,5] Diffusion-driven mass transport between γ' precipitates and γ matrix affects the ordering and dissolution behavior of the γ' precipitates and thus the mechanical properties. Fundamental studies on the solute redistribution and microstructure evolution of the γ/γ' system under heat treatments are crucial to understand their behavior for the high-temperature applications.

Diffusion of alloy components is significantly influenced by the state of ordering.[6] In disordered solid solution alloys, diffusion typically occurs through the random walk of thermal vacancies. In ordered intermetallic, the random walk of vacancies can disrupt the equilibrium ordering arrangement of atoms. However, diffusion through nonrandom motion of vacancies allows the atom–vacancy exchanges to take place without sacrificing long-range ordering.[7] In $L1_2$-structured Ni_3Al, there are two major self-diffusion mechanisms proposed. One view holds that Ni atoms diffuse through site exchanges with a neighboring vacancy on its own sublattice without concomitant disordering, where a six-jump vacancy sequence may be operative with Ni and Al moving simultaneously during diffusion.[8] Another perspective is that the minor element, Al, occupying lattice sites of the sublattice of the major atoms (i.e. Ni) can diffuse through the Ni-sublattice.[9] Watanabe et al. studied the interdiffusion in a Ni/Ni_3Al diffusion couple and pointed out that the interdiffusivities follow the modified Darken's equation.[10]

The nucleation of γ' precipitates is normally considered as a diffusional transformation and occurs through classic nucleation and growth mechanism. In the theory of nucleation, the precipitation of a second phase can result in the reduction of total free energy of the system and the rate of precipitation significantly depends on the temperature of undercooling at which the precipitation initiates.[11] The coarsening of γ' precipitates in the γ matrix is a diffusion-driven Ostwald ripening process.[12–16] During heat treatment, the interfacial energy can provide a driving force for

*Corresponding author. Emails: csun@lanl.gov, chengsun2008@gmail.com

coarsening and morphological changes of γ' precipitates, which in turn results in a reduction of total interfacial energy.[12,17] The morphological change of γ' precipitates is significantly influenced by the elastic energy associated with the lattice parameter misfit between the matrix and the precipitate.[18] In misfit-free (matrix and precipitate) Ni–Cr–Al alloys, γ' precipitates grow as spheres as predicted by the Lifshitz–Slyozov–Wagner (LSW) theory.[19–21] With increasing misfit between the matrix and the precipitate, by the addition of molybdenum for instance, the morphology of γ' precipitates in a Ni–Cr–Al–Mo alloy changed from spheroidal to cuboidal.[22]

Pristine defects in the components have an important impact on the coarsening kinetics of γ' precipitates.[23,24] High-angle grain boundaries are considered as solute diffusion paths contributing to the growing of precipitates that are located on grain boundaries. Dislocations intersecting the precipitate surface can generate fast pipe diffusion and thus serve as paths for precipitate coarsening.[23] Here, we used Ni/Ni_3Al as a γ/γ' model system to explore the role of interfaces on precipitation and the competing tendencies to order and dissolve the supersaturated Ni_3Al layer. Interface promotes the formation of γ' precipitates due to the preferential vacancy diffusion along the interface.

2. Experiments and Modeling Methodologies

Ni/Ni_3Al multilayers were synthesized by magnetron sputtering at 500°C under vacuum at a pressure of 3×10^{-3} torr. The base pressure of the system was 1×10^{-8} torr. The first Ni layer with a thickness of 100 nm was deposited on an MgO substrate, the second Ni_3Al layer with a thickness of 200 nm was cosputtered from Al and Ni targets, and the third layer was the Ni–Al cap layer ($\sim$100 nm in thickness). The DC power used on the targets was varied as necessary to achieve the required stoichiometry. After deposition, Ni/Ni_3Al films were annealed at 800°C for 1 h with gettered Ar flowing through the tube and cooled down to room temperature at a controlled rate of 5°C/min. Cross-sectional samples were prepared for transmission electron microscopy (TEM) observation by mechanical polishing followed by subsequent ion-milling.

TEM was performed on an image-corrected FEI Titan at Los Alamos National Laboratory (LANL), operated in TEM mode at 300 keV. To acquire structural high-angle annular dark- and bright-field images, the 200 keV JEOL ARM at Arizona State University was utilized to perform scanning transmission electron microscopy (STEM). Spectral imaging was utilized to acquire the Ni-L and Al-K near-edge fine structures with the best achievable spatial and energy resolution for each microscope. Particular attention was paid to minimize the effects of electron irradiation on the sample materials, to assure that all the reported results are not a consequence of electron-beam-induced damage, by utilizing lower dose imaging techniques.

An off-lattice kinetic Monte Carlo algorithm [25,26] was used to study the Ni_3Al precipitation process in the presence of misfit strain. One vacancy was introduced in the system and its exchange rates can be calculated by using Glauber dynamics, that is,

$$r_j = \frac{x_j}{1 + x_j}, \tag{1}$$

$$x_j = \exp\left\{\frac{-\Delta E_j}{kT}\right\}, \tag{2}$$

where ΔE_j is the change in energy between the final and initial configurations. The pressure of the sample was relaxed every 100 Monte Carlo steps to take into account the internal strain fields due to lattice mismatch. Periodic boundary conditions were applied in every dimension. Once the rates were calculated, the traditional Bortz–Kalos–Lebowitz (BKL) algorithm [27] was used to study the evolution of the microstructure using the rates as defined in Equation (2). The embedded-atom method (EAM) potential developed by Mishin [28] was used to calculate ΔE_j, as, in our experience, it best reproduces the experimental phase diagram. This algorithm does not capture the dynamics of the process, but elucidates the most important effects in the competition between ordering and interdiffusion. In particular, because prefactors and barriers for each rate are not calculated, the 'time scale' is not representative of the experiment, but the trajectories should be reasonable.

3. Results and Discussion

Figure 1 shows the microstructure of the as-deposited Ni/Ni_3Al film. Figure 1(a) shows the bright-field TEM image and the inset selected area electron diffraction (SAED) pattern obtained along the [100] zone axis, containing MgO substrate, Ni, and Ni_3Al layers. The inset SAED pattern shows that the Ni_3Al layer was a chemically partially ordered structure due to the presence of intense diffraction maxima at the ⟨110⟩ orientation. Complementary energy dispersive X-ray spectroscopy (EDS) line scans were performed across the film (Figure 1(b)). A Ni layer with the thickness of $\sim$100 nm and a $Ni_{0.73}Al_{0.27}$ layer of $\sim$200 nm were resolved. Figure 1(c) shows the bright-field TEM image under kinematic imaging conditions with a diffraction vector $g = [110]$. To image the precipitates, dark-field TEM images were taken as shown in Figure 1(d). The bright columnar structure in the Ni_3Al layer in Figure 1(d) was identified as the γ' (Ni_3Al in $L1_2$ structure) phase. Interestingly, some isolated nanometric γ' particles were formed on the Ni/Ni_3Al interface during the deposition at 500°C, as marked by the arrows in Figure 1(d).

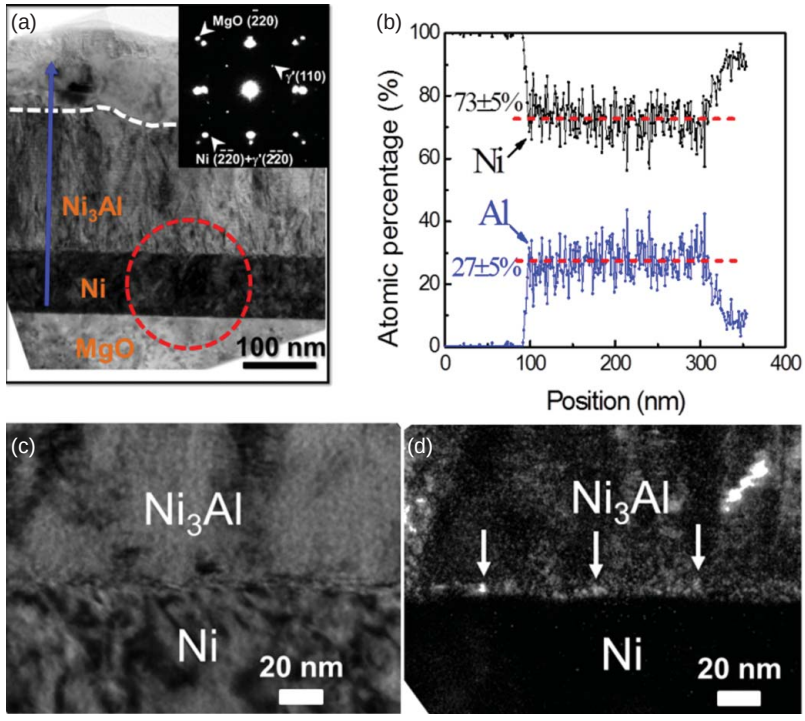

Figure 1. (a) TEM images obtained from the as-deposited pristine Ni/Ni_3Al thin-film multilayer on an MgO substrate. SAED pattern was taken from the circled area, including the MgO substrate, Ni, and Ni_3Al layers. Superlattice reflections, as indicated in the inset, suggest an ordered structure in the Ni_3Al layer. (b) EDS line scan across the film. The average ratio of Ni to Al concentration is measured to be 73%:27%. (c) Bright-field TEM image of the as-deposited Ni/Ni_3Al film. (d) Dark-field image with diffraction vector $g = [110]$, showing columnar γ' (Ni_3Al) precipitate phase in the Ni_3Al layer and some isolated nanoscaled γ' (Ni_3Al) particles formed on the Ni/Ni_3Al interface.

After annealing at 800°C for 1 h, the sample homogenized and no clear interfaces were observed (Figure 2(a)). The SAED pattern obtained from the annealed film suggests long-range ordering. A complementary EDS line scan performed across the film in Figure 2(b) shows a slight gradient in the Ni and Al compositions. Supplementary Figure S1 shows the microstructure of an as-annealed sample. The γ' precipitates appear as bright spots and these precipitates were formed throughout the film. A high-resolution STEM image obtained from the annealed film, shown in Figure 2(c), highlighted the Z-contrast difference between the matrix and the precipitates. Fast Fourier Transformed (FFT) diffraction patterns from selected regions of the STEM image suggested that these regions were composed of a disordered fcc-structured γ matrix and an ordered $L1_2$-structured γ' precipitates. Figure 2(d) shows a bright-field TEM image of a local area in the annealed film. A magnified annular bright-field (ABF) image of the area outlined by the box is shown in Figure 2(e), revealing a high density of precipitates (dark contrast features). Figure 2(f) and 2(g) shows STEM-based EDS chemical mappings of Ni and Al; interpretation of the EDS maps suggests the enrichment of Al in γ' precipitates. X-ray powder diffraction (XRD) profiles of the Ni/Ni_3Al film before and after annealing are shown in Figure S2. In the as-deposited state, the lattice parameters (a) of Ni and Ni_3Al were measured to be 3.552 and 3.561 Å, respectively, and thus the misfit strain (ε) was $\sim$0.25%, estimated by $\varepsilon = \Delta a/a$. After annealing, due to the intermixing of Ni and Al across the film and the greater amount of $L1_2$ precipitation, the lattice parameter of the matrix ($Ni_{80}Al_{20}$) and the precipitates (Ni_3Al) became 3.542 and 3.583 Å, respectively, and the misfit strain was $\sim$1.16%. Comparing the XRD profiles in Figure S2, more superlattice peaks, such as Ni_3Al (111) and Ni_3Al (210), were observed in the as-annealed state, which implies the evolution of texture, where grains with different orientations are formed.

The above observations lead to the following picture for the evolution of precipitates in the γ/γ' system under thermal annealing. In the Ni layer, the diffusion of Al from the Ni_3Al layer first leads to the formation of a Ni–Al solid solution. As the interdiffusion extends, γ' precipitates are nucleated due to the supersaturation of Al. In the Ni_3Al layer, the initial γ' phase evolves into nanometer-sized γ' precipitates under annealing. The partitioning of the elements Ni and Al causes changes in the lattice parameter of the matrix, and therefore changes the lattice mismatch between the matrix and the precipitates. The loss of Al and the gain of Ni in the Ni_3Al layer result in the increase of mismatch strain between the γ'

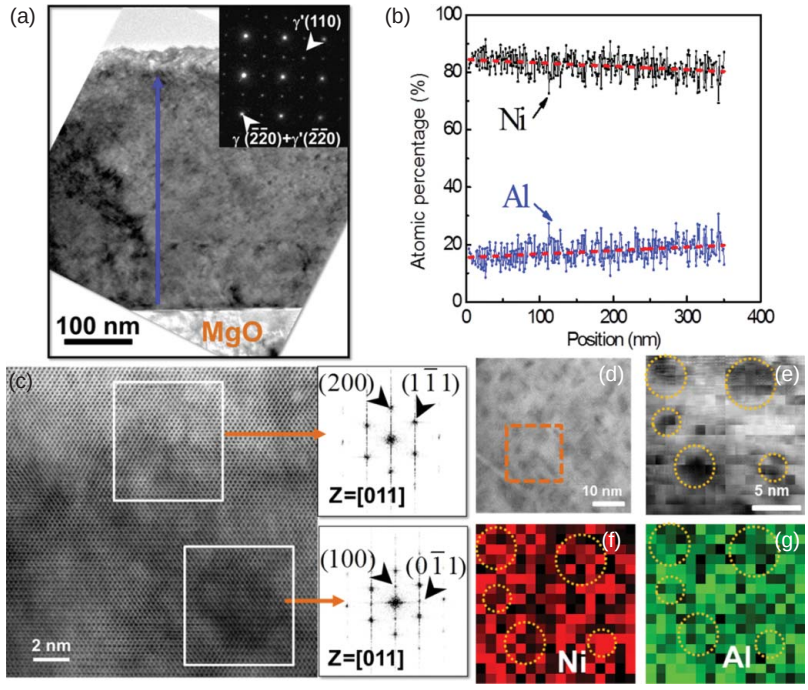

Figure 2. (a) Bright-field TEM image of the as-annealed film, showing no clear Ni/Ni_3Al interfaces. The inset SAED pattern shows an ordered structure of the film. (b) Measured chemical profile of the film after annealing. Thermally induced chemical intermixing over the entire film occurs under annealing. (c) High-resolution STEM image showing atomic (Z) contrast in a local area of the annealed sample. FFT patterns show clear evidence of a disordered matrix and ordered precipitates. (d) Bright-field TEM image in a local area, showing a high density of precipitates. (e) High-resolution STEM annual bright-field (STEM-ABF) image obtained from the area within the box in (d). Precipitates are marked with circles. (f and g) High-resolution EDS mapping of Ni and Al distribution in (e).

precipitates and the matrix. The increase in the lattice mismatch can also induce changes in the morphology of the γ' precipitates. For the small γ' precipitates, the morphology tends to be spherical in order to minimize the interfacial energy, while for the large γ' precipitates, as the strain energy increases, the shape of the precipitates evolves into platelets or facets.[18] In our current study, both spherical and plate-like precipitates form in the matrix after thermal annealing, as shown in Figure 2(d).

Bright-field TEM images were collected near the Ni/Ni_3Al interface of the as-annealed sample, as shown in Figure 3(a). Compared with the precipitates in the matrix, the size of the precipitates became larger and the geometry of these precipitates became faceted, as shown in Figure 3(b). STEM images of the as-deposited and as-annealed samples are shown in Figure S3, and the comparison reveals that the precipitates formed at the interface exhibited a lower mass contrast. A high-resolution EDS line scan across the precipitate is plotted in Figure 3(c). From the EDS line scan it can be seen that the precipitates had a higher concentration of Al and lower concentration of Ni compared with the background matrix; the atomic concentration ratio of Ni to Al in the precipitates was close to 3:1. Figure 3(d) shows a high-resolution STEM image of the phase boundary between the matrix and a precipitate. The Z-contrast imaging near the phase boundary suggests aggregation of Al in the precipitate, which is consistent with the measured chemical profile of γ' precipitates studied with EDS. Statistical analysis was performed on the measured sizes of precipitates in the annealed sample. The results of this analysis are presented in Figure 3(e) and 3(f) and show that the average precipitate size was $\sim$11 nm in the vicinity of the original parent interface, which was $\sim$2.8 times larger than that of the precipitates in the matrix. Annealing twins observed between Ni/Ni_3Al and Ni/MgO interfaces, as shown in Figure S4, might be the result of interface relaxation during heat treatment.

To better understand the role of the interface in enhancing the precipitation of γ', we used kinetic Monte Carlo to model the evolution of a fully coherent Ni/Ni_3Al interface under thermal annealing. One sample oriented in the direction [100], [010], and [001] was generated with dimensions 4.3 nm $\times$ 4.3 nm $\times$ 14.2 nm containing 23,040 atoms (Figure S5). The figure shows only Ni atoms that have eight Ni and four Al first-nearest neighbors and Al atoms with 12 Ni first-nearest neighbors; these are the environments that belong to an $L1_2$ structure. A vacancy was added randomly to the sample and evolved as described in the Methods section. Figure 4 shows the microstructural evolution of the system at

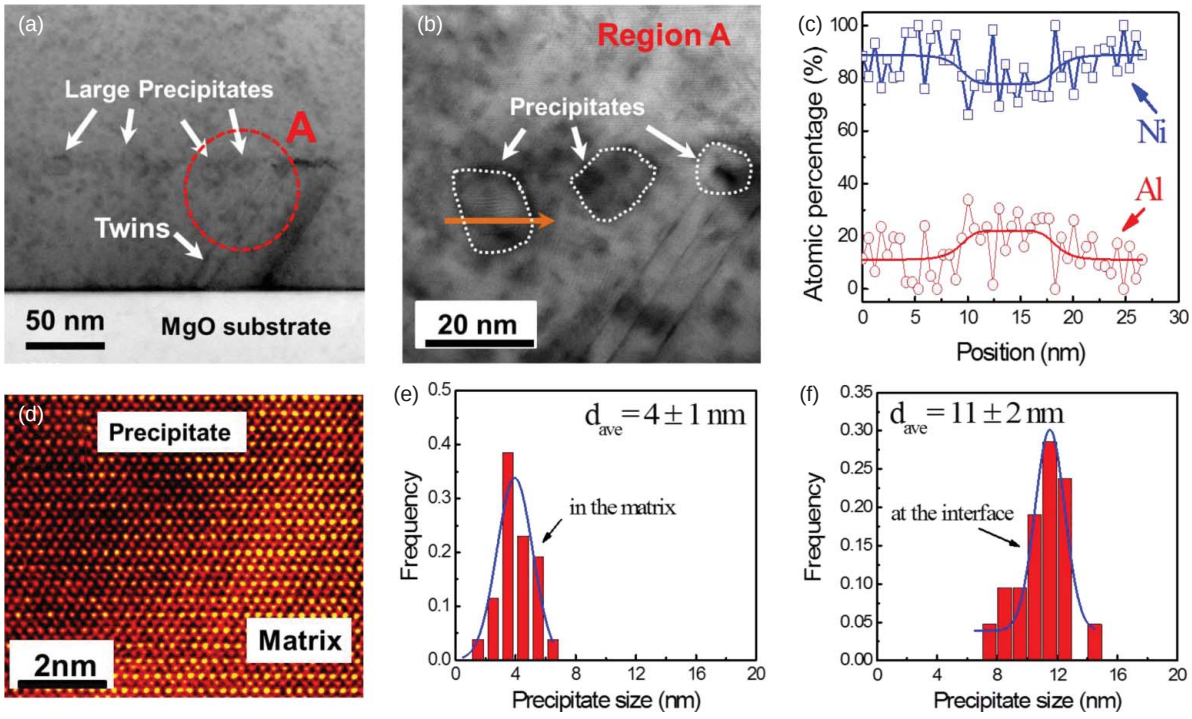

Figure 3. (a) Bright-field STEM image of the precipitates within the annealed sample located near the parent Ni/Ni_3Al interface. Larger sized precipitates and annealing twins were formed. (b) Magnified STEM micrograph of region 'A' showing large faceted precipitates. (c) High-resolution line scan across the precipitate marked by the orange arrow in (b). The atomic percent ratio of Ni to Al within the precipitate is ~3:1. (d) High-resolution STEM image of the precipitate/matrix showing a coherent interface was formed. (e) The average size of the precipitates in the matrix is measured to be ~4 nm. (f) The average size of the precipitates near the parent Ni/Ni_3Al interface is ~11 nm.

500°C, mimicking the deposition conditions, as given by the Monte Carlo simulations at different time steps, 3.60×10^5, 7.00×10^5, and 1.17×10^6. Figure 4(a), 4(d), and 4(g) shows the atomic configuration of the system at different stages. It is clear that ordering occurs in the system with the nucleation and growth of $L1_2$ precipitates. We also analyzed the distribution of Al in the sample and the average of the vacancy position along 10^5 Monte Carlo steps with the average steps. Figure 4(b), 4(e), and 4(h) shows these results, with the blue dashed curve displaying the Al distribution and the black curve showing the vacancy probability. Two main results can be extracted from these calculations: (1) The vacancy spends most of the time close to the interface (within the Ni-rich region). (2) There is Al intermixing into the Ni-rich layer that does not lead to the formation of $L1_2$ (over the length of the simulations studied) while ordering occurs in the Al supersaturated region. Figure 4(c), 4(f), and 4(i) describe the Al content belonging to an $L1_2$ structure. We observe the development of a peak close to one of the interfaces, where the vacancy spends most of the time (note that periodic boundary conditions were applied). Shaded regions are used as guides to the eye that show the Al undersaturated regions. These results show that the interface plays an important role in the formation of γ' precipitates, increasing the propensity for the formation of these precipitates along the Ni/Ni_3Al interface. The longer time that the vacancy spends at the interface enhances the nucleation of γ' precipitates. This is particularly interesting as, in this model, there are no misfit dislocations at the interface—it is fully coherent. Thus, even a coherent interface leads to trapping of the vacancy and enhanced precipitation. We expect the effect to be even more dramatic when dislocations are present.

Based on the aforementioned experimental and simulation studies, we can conclude that the γ' particles are favorably formed on the Ni/Ni_3Al interface during the deposition at 500°C as a result of the enhanced vacancy diffusion along the interface. Under thermal annealing at 800°C, the interface gradually becomes invisible due to the interdiffusion of Ni and Al across the interface, and the γ' precipitates in the vicinity of the parent interface grow much faster compared to those nucleated in the matrix because of the trapping of vacancies by the interface. In addition, the Monte Carlo simulation implies that the interface between the γ' precipitates and the γ matrix may also serve as the vacancy diffusion path and promote the coarsening of the γ' precipitates.

4. Conclusions Interdiffusion and precipitation behavior in a model γ/γ' system were studied by an

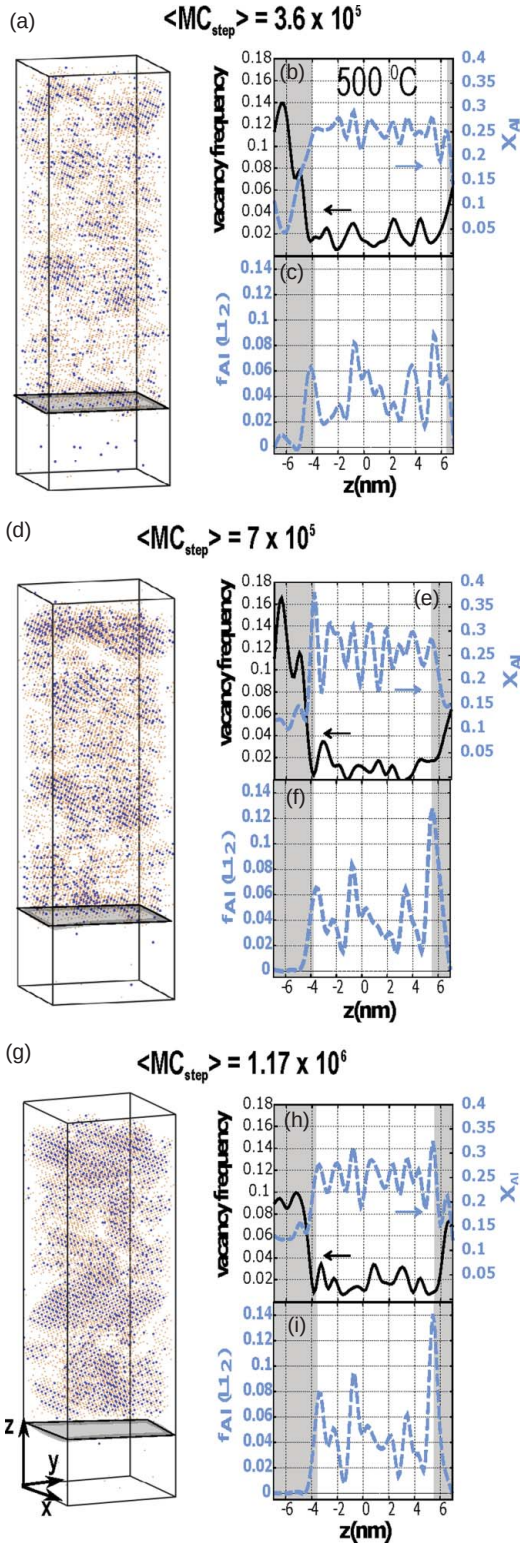

Figure 4. (a), (d), and (g) Distribution of Ni and Al atoms (brown and blue, respectively) in $L1_2$ structure at 500°C after 3.60×10^5, 7.00×10^5, and 1.17×10^6 steps, respectively. The original structure has two sharp Ni/Ni_3Al interfaces, one at the top boundary of the cell, and one at about one-fifth of the cell dimension from the bottom. (b), (e), and (h) show the average vacancy frequency in the z direction (black) and the total Al distribution (blue) for the different Monte Carlo steps. (c), (f), and (g) show the fraction of Al in the $L1_2$ structure for the different steps. Shaded areas show the approximate width of the Al undersaturated region.

experiment and Monte Carlo simulations. Interdiffusion, induced by thermal annealing, of the elements Ni and Al across the Ni/Ni_3Al interface resulted in the disappearance of the parent interface. Under thermal annealing at 800°C, ordered γ' precipitates with an average size of $\sim$4 nm were formed throughout the film sample and larger γ' precipitates with an average size of $\sim$11 nm were created near the parent Ni/Ni_3Al interface. The pristine Ni/Ni_3Al interface promotes the formation of the γ' precipitates. Vacancies preferentially diffuse along the interface, accelerating the precipitation of Ni_3Al particles. Our current study shows that the Ni/Ni_3Al interface has pronounced impact on the γ' precipitation during thermal annealing, suggesting the importance of an interface design in Ni-based superalloys for high-temperature applications.

Acknowledgements We acknowledge the financial support by LDRD program in Los Alamos National Laboratory. Los Alamos National Laboratory is operated by Los Alamos National Security, LLC, for the National Nuclear Security Administration of the U.S. DOE under contract DE-AC52-06NA25396. We thank Dr Robert Dickerson for helpful discussions. We also acknowledge that parts of the TEM work were performed at the LeRoy Eyring Center for High Resolution Electron Microscopy at Arizona State University (ASU) in collaboration with Toshihiro Aoki, and some of the high-resolution STEM work was conducted at the Center for Nanophase Materials Science, which is a DOE Office of Science User Facility.

Disclosure Statement No potential conflict of interest was reported by the authors.

Supplementary Online Material A more detailed information on experiments is available at http://dx.doi.org/10.1080/21663831.2015.1045630.

References

[1] Pollock TM, Tin S. Nickel-based superalloys for advanced turbine engines: chemistry, microstructure and properties. J Propul Power. 2006;22:361–374.
[2] Furrer D, Fecht H. Ni-based superalloys for turbine discs. JOM. 1999;51:14–17.
[3] Unocic R, Viswanathan G, Sarosi P, Karthikeyan S, Li J, Mills M. Mechanisms of creep deformation in polycrystalline Ni-base disk superalloys. Mater Sci Eng A. 2008;483–484:25–32.
[4] Caron P. High γ' solvus new generation nickel-based superalloys for single crystal turbine blade applications. In: Pollock TM, Kissinger RD, Bowman RR, Green KA, McLean M, Olson S, Schirra JJ, editors. Superalloys. Warrendale, PA: The Minerals, Metals & Materials Society; 2000. p. 737–746.
[5] Payton EJ, Phillips PJ, Mills MJ. Semi-automated characterization of the phase in Ni-based superalloys via high-resolution backscatter imaging. Mater Sci Eng A. 2010;527:2684–2692.
[6] Mehrer H. Diffusion in intermetallics. Mater Trans JIM. 1996;37:1259–1280.
[7] Yasuda HY, Nakajima H, Koiwa M. Diffusion in L12-type intermetallic compounds. Defect Diffus Forum. 1993;95–98:823–830.

[8] Nakajima H, Nonaka K, Sprengel W, Koiwa M. Self-diffusion and interdiffusion in intermetallic compounds. Mater Sci Eng A. 1997;239–240:819–827.
[9] Koiwa M, Numakura H, Ishioka S. Diffusion in L12 type intermetallic compounds. Defect Diffus Forum. 1997;143–147:209–222.
[10] Watanabe M, Horita Z, Sano T, Nemoto M. Electron microscopy study of Ni/Ni_3Al diffusion-couple interface—II. Diffusivity measurement. Acta Metall. 1994;42:3389–3396.
[11] Svoboda J, Fischer FD, Fratzl P, Kozeschnik E. Modelling of kinetics in multi-component multi-phase systems with spherical precipitates: I: theory. Mater Sci Eng A. 2004;385:166–174.
[12] Baldan A. Review progress in Ostwald ripening theories and their applications to nickel-base superalloys Part I: Ostwald ripening theories. J Mater Sci. 2002;37:2171–2202.
[13] Wendt h, Haasen P. Nucleation and growth of γ'-Precipitates in Ni-14 at.% Al. Acta Metall. 1983;31:1649–1659.
[14] Hirata T, Kirkwood DH. The prediction and measurement of precipitate number densities in a nickel-6.05 wt.% aluminium alloy. Acta Metall. 1977;25:1425–1434.
[15] Ges A, Fornaro O, Palacio H. Long term coarsening of γ' precipitates in a Ni-base superalloy. J Mater Sci. 1997;32:3687–3691.
[16] Ma Y, Ardell AJ. Coarsening of γ (Ni–Al solid solution) precipitates in a γ' (Ni_3Al) matrix. Acta Mater. 2007;55:4419–4427.
[17] Maebashi T, Doi M. Coarsening behaviours of coherent γ' and γ precipitates in elastically constrained Ni–Al–Ti alloys. Mater Sci Eng A. 2004;373:72–79.
[18] Gleiter H, Hornbogen E. Precipitation hardening by coherent particles. Mater Sci Eng. 1968;2:285–302.
[19] Lifshitz IM, Slyozov VV. The kinetics of precipitation from supersaturated solid solutions. J Phys Chem Solids. 1961;19:35–50.
[20] Greenwood GW. The growth of dispersed precipitates in solutions. Acta Metall. 1956;4:243–248.
[21] Wagner C. The determination of small deviations from the ideal stoichiometric composition of ionic crystals and other binary compounds. Prog Solid State Chem. 1971;6:1–15.
[22] Loomis W, Freeman J, Sponseller D. The influence of molybdenum on the γ' phase in experimental nickel-base superalloys. Metall Trans. 1972;3:989–1000.
[23] Jayanth CS, Nash P. Factors affecting particle-coarsening kinetics and size distribution. J Mater Sci. 1989;24:3041–3052.
[24] Hin C. Kinetics of heterogeneous grain boundary precipitation of Ni 3 Al in nickel alloy. J Phys D Appl Phys. 2009;42:225309.
[25] Sadigh B, Erhart P, Stukowski A, Caro A, Martinez E, Zepeda-Ruiz L. Scalable parallel Monte Carlo algorithm for atomistic simulations of precipitation in alloys. Phys Rev B. 2012;85:184203.
[26] Martínez E, Caro A. Atomistic modeling of long-term evolution of twist boundaries under vacancy supersaturation. Phys Rev B. 2012;86:214109.
[27] Bortz AB, Kalos MH, Lebowitz JL. A new algorithm for Monte Carlo simulation of Ising spin systems. J Comput Phys. 1975;17:10–18.
[28] Mishin Y. Atomistic modeling of the γ and γ'-phases of the Ni–Al system. Acta Mater. 2004;52:1451–1467.